Supplementary Information

A Novel Monoclonal Antibody Targeting a Large Surface of the Receptor Binding Motif Shows Pan-neutralizing SARS-CoV-2 Activity Including BQ.1.1 Variant

Leire de Campos-Mata, Benjamin Trinité, Andrea Modrego, Sonia Tejedor Vaquero, Edwards Pradenas, Natalia Rodrigo Melero, Diego Carlero, Silvia Marfil, Anna Pons-Grífols, María Teresa Bueno-Carrasco, César Santiago, Ferran Tarrés-Freixas, Victor Urrea, Nuria Izquierdo, Eva Riveira-Muñoz, Ester Ballana, Mónica Pérez, Júlia Vergara-Alert, Joaquim Segalés, Carlo Carolis*, Rocío Arranz*, Julià Blanco*, Giuliana Magri*

*Corresponding authors:

Carlo Carolis, carlo.carolis@crg.eu;

Rocío Arranz, rarranz@cnb.csic.es;

Julià Blanco, jblanco@irsicaixa.es;

Giuliana Magri, gmagri@imim.es

This file includes:

Supplementary Figures and legends 1-5
Supplementary Tables 1-4

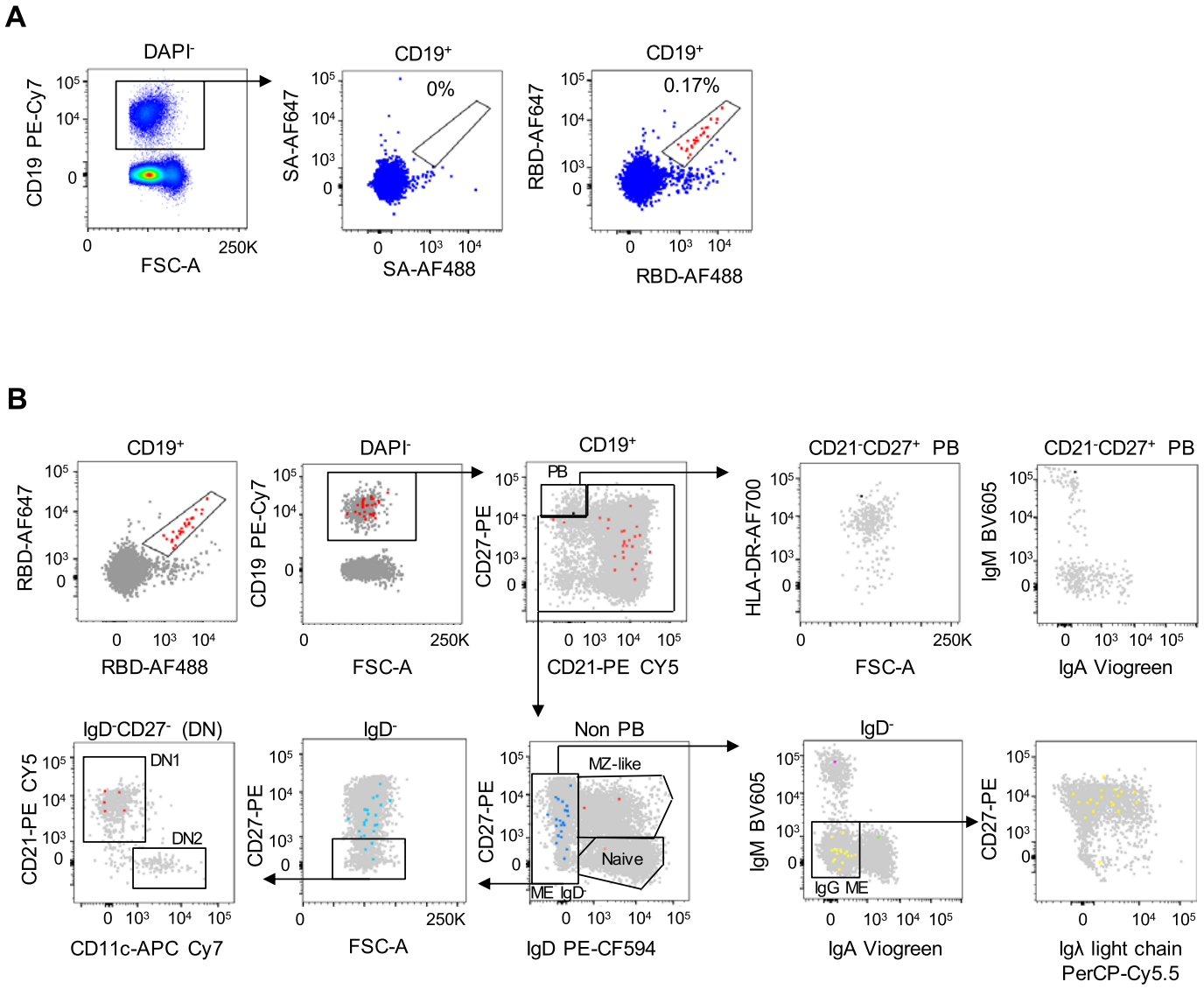
A
DAPI-
CD19 PE-Cy7
FSC-A
250K
CD19+
SA-AF647
SA-AF488
0%
CD19+
RBD-AF647
RBD-AF488
0.17%
B
CD19+
RBD-AF647
RBD-AF488
DAPI-
CD19 PE-Cy7
FSC-A
250K
CD19+
PB
CD27-PE
CD21-PE CY5
CD21-CD27+ PB
HLA-DR-AF700
FSC-A
CD21-CD27+ PB
IgM BV605
IgA Viogreen
IgD-CD27- (DN)
DN1
DN2
CD21-PE CY5
CD11c-APC Cy7
IgD-
CD27-PE
FSC-A
250K
Non PB
MZ-like
Naive
ME IgD-
CD27-PE
IgD PE-CF594
IgD-
IgM BV605
IgG ME
IgA Viogreen
CD27-PE
Igλ light chain
PerCP-Cy5.5

Supplementary Figure 1. Characterization SARS CoV-2 WH1 RBD-specific B cells by flow cytometry. **(A)** Flow cytometry staining of $CD19^+$ B cells from a convalescent COVID-19 individual without (left) and with (right) two fluorescently labeled biotinylated RBD probes. Numbers indicate the percentage of RBD-specific cells within total $CD19^+$ B cells. Red large dots represent cells that are positive for both RBD-AF647 and RBD-AF488. **(B)** Gating strategy used to define RBD-specific B cell populations: PBs ($CD19^+CD27^{++}CD21^-$), MZ-like (non-PB $CD19^+CD27^+IgD^+$), naïve (non-PB $CD19^+CD27^-IgD^+$), ME IgD^- (non-PB $CD19^+IgD^-$), IgM^+ ME (non-PB $CD19^+IgD^-IgM^+$), IgA^+ ME (non-PB $CD19^+IgD^-IgA^+$), IgG^+ ME (non-PB $CD19^+IgD^-IgG^+$), DN1 (non-PB $CD19^+IgD^-CD27^-CD21^+CD11c^-$), and DN2 (non-PB $CD19^+IgD^-CD27^-CD21^-CD11c^+$). RBD-specific cells are represented in colored large dots.

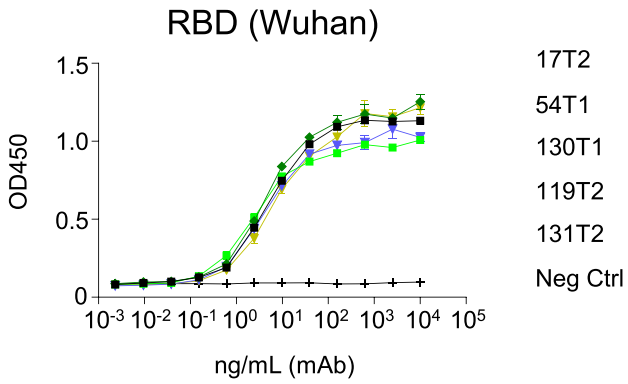
RBD (Wuhan)
OD450
1.5
1.0
0.5
0
10-3 10-2 10-1 100 101 102 103 104 105
ng/mL (mAb)
17T2
54T1
130T1
119T2
131T2
Neg Ctrl

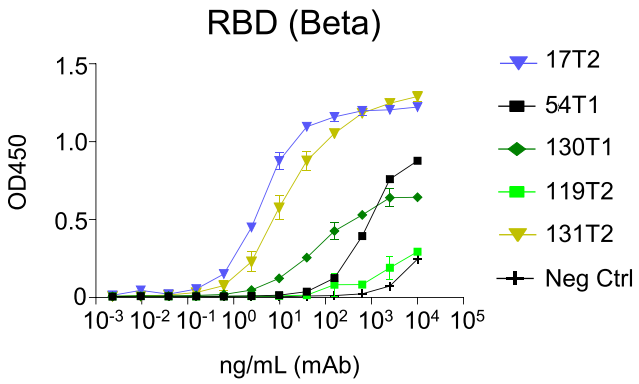
RBD (Beta)
OD450
1.5
1.0
0.5
0
10-3 10-2 10-1 100 101 102 103 104 105
ng/mL (mAb)
17T2
54T1
130T1
119T2
131T2
Neg Ctrl

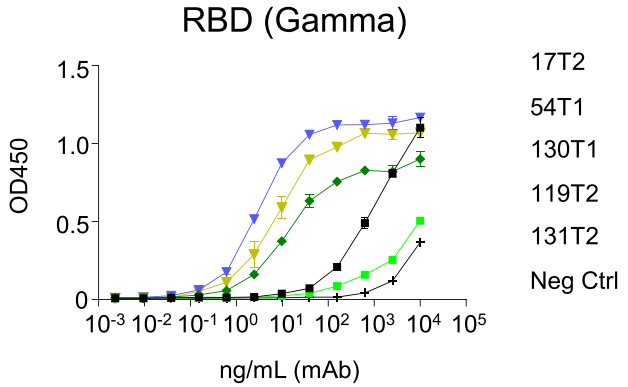
RBD (Gamma)
OD450
1.5
1.0
0.5
0
10-3 10-2 10-1 100 101 102 103 104 105
ng/mL (mAb)
17T2
54T1
130T1
119T2
131T2
Neg Ctrl

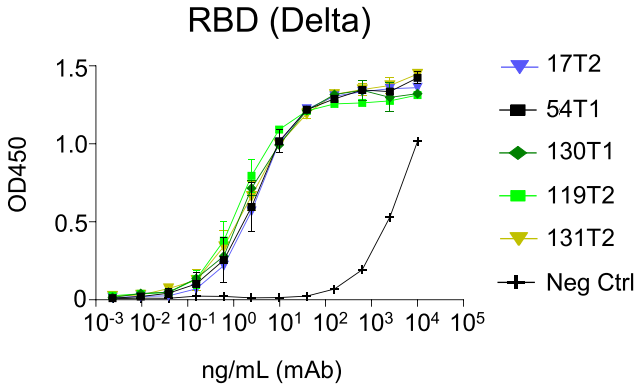
RBD (Delta)
OD450
1.5
1.0
0.5
0
10-3 10-2 10-1 100 101 102 103 104 105
ng/mL (mAb)
17T2
54T1
130T1
119T2
131T2
Neg Ctrl

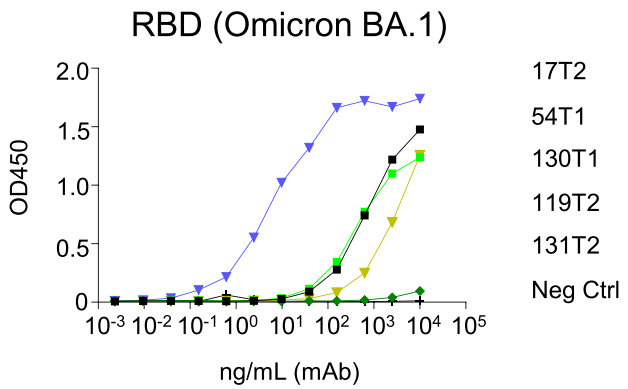
RBD (Omicron BA.1)
OD450
2.0
1.5
1.0
0.5
0
10-3 10-2 10-1 100 101 102 103 104 105
ng/mL (mAb)
17T2
54T1
130T1
119T2
131T2
Neg Ctrl

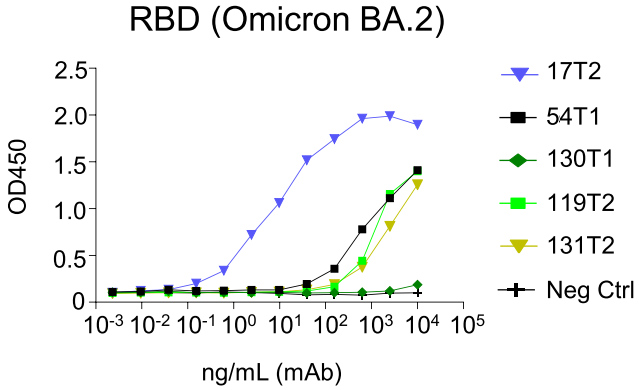
RBD (Omicron BA.2)
OD450
2.5
2.0
1.5
1.0
0.5
0
10-3 10-2 10-1 100 101 102 103 104 105
ng/mL (mAb)
17T2
54T1
130T1
119T2
131T2
Neg Ctrl

Supplementary Figure 2. Reactivity of SARS-CoV-2 RBD-specific monoclonal antibodies. ELISA binding curves of serial dilutions of the mAbs to the spike RBD of SARS-CoV-2 from different variants, coated at equimolar concentrations. Graph bars represent the average ± SD. Human IgG1 purified from serum of a myeloma patient (binding site company, BP078) was used as a negative control for binding.

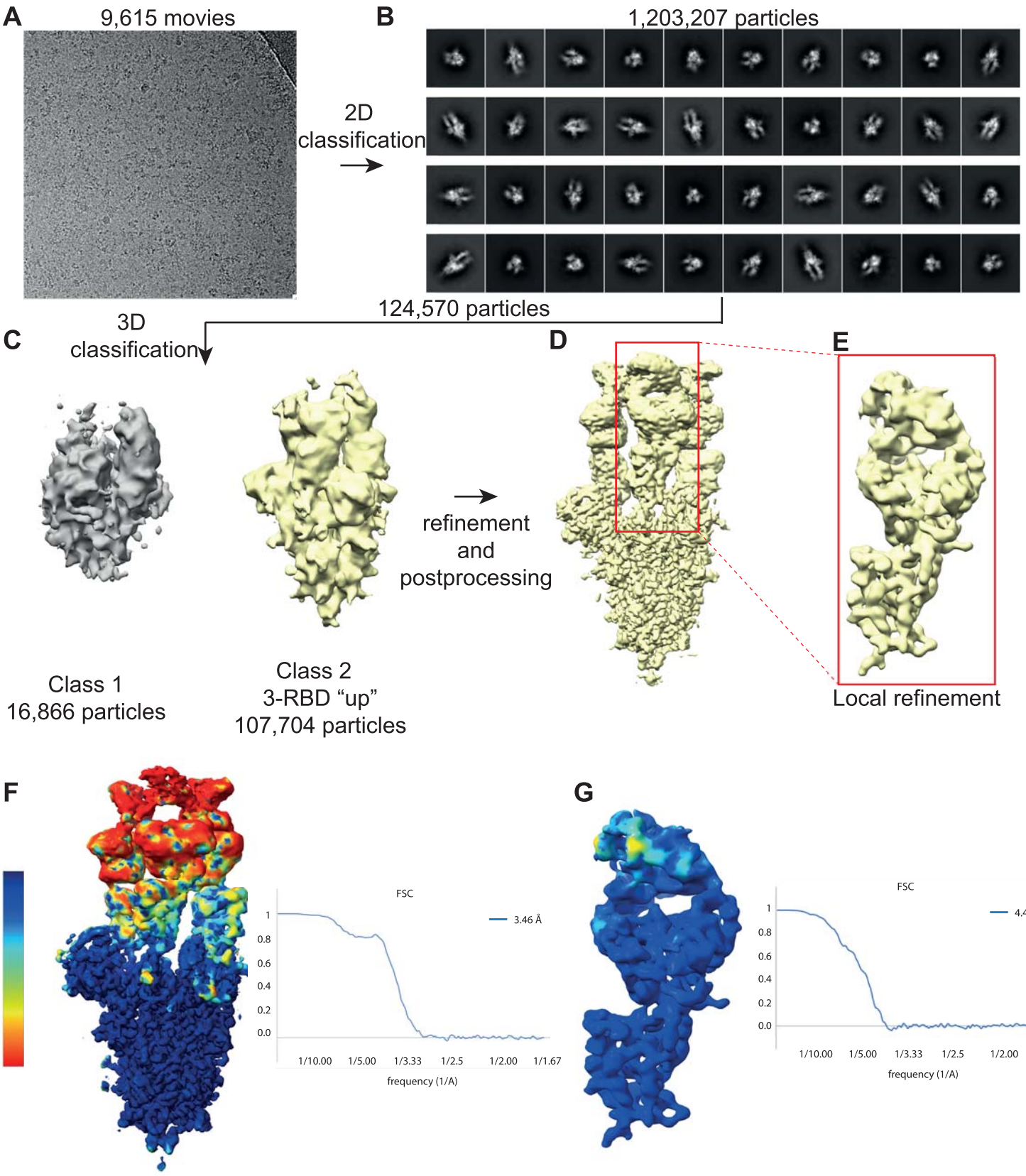
A
9,615 movies
B
1,203,207 particles
2D
classification
124,570 particles
3D
classification
C
Class 1
16,866 particles
Class 2
3-RBD “up”
107,704 particles
refinement
and
postprocessing
D
E
Local refinement
F
3.5
4.8
6.1
7.4
8.7
10.0
FSC
3.46 Å
1
0.8
0.6
0.4
0.2
0.0
1/10.00
1/5.00
1/3.33
1/2.5
1/2.00
1/1.67
frequency (1/A)
G
FSC
4.41 Å
1
0.8
0.6
0.4
0.2
0.0
1/10.00
1/5.00
1/3.33
1/2.5
1/2.00
1/1.67
frequency (1/A)

Supplementary Figure 3. Cryo-EM data analysis for complex between the Omicron BA.1 spike trimer and the 17T2 Fab fragment. **(A)** Representative electron micrograph. **(B)** Representative 2D-class averages. **(C)** 3D classification. Left class contains low quality particles and right class contains high quality particles that were selected for refinement. **(D)** 3D reconstruction of complex with no symmetric imposed. **(E)** The boxed region contains one RBD complexed with one Fab in a refined map masked by local refinement. **(F-G)** Gold standard Fourier shell correlation (FSC) curve of final overall (left) and locally refined (right) maps and resolution estimation based on 0.143 Fourier shell correlation criteria as indicated by a blue line.

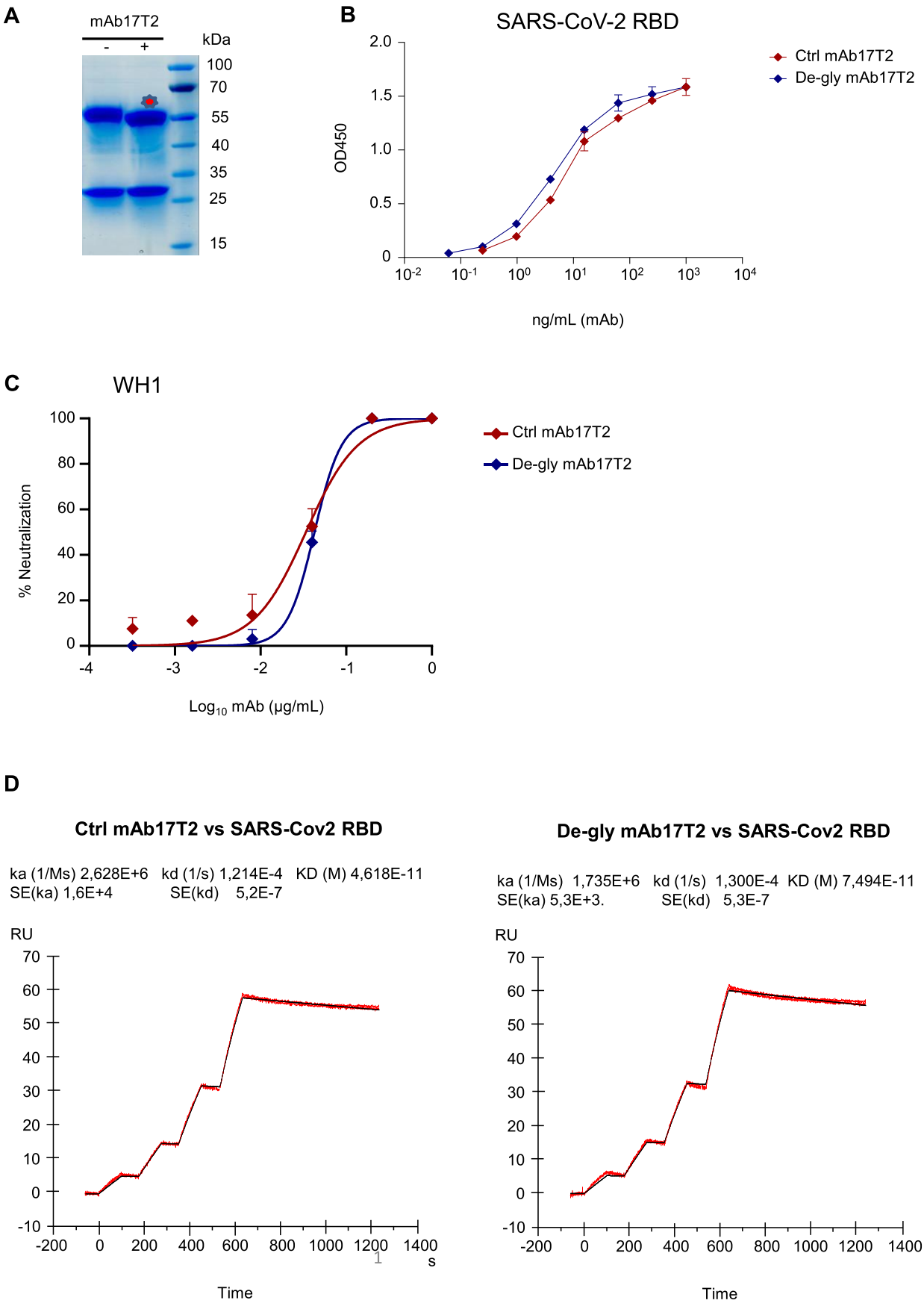
A
mAb17T2
-
+
kDa
100
70
55
40
35
25
15
B
SARS-CoV-2 RBD
OD450
2.0
1.5
1.0
0.5
0
10^{-2}
10^{-1}
10^{0}
10^{1}
10^{2}
10^{3}
10^{4}
ng/mL (mAb)
Ctrl mAb17T2
De-gly mAb17T2
C
WH1
% Neutralization
100
80
60
40
20
0
-4
-3
-2
-1
0
Log_{10} mAb (µg/mL)
Ctrl mAb17T2
De-gly mAb17T2
D
Ctrl mAb17T2 vs SARS-Cov2 RBD
ka (1/Ms) 2,628E+6 kd (1/s) 1,214E-4 KD (M) 4,618E-11
SE(ka) 1,6E+4 SE(kd) 5,2E-7
RU
70
60
50
40
30
20
10
0
-10
-200
0
200
400
600
800
1000
1200
1400
s
Time
De-gly mAb17T2 vs SARS-Cov2 RBD
ka (1/Ms) 1,735E+6 kd (1/s) 1,300E-4 KD (M) 7,494E-11
SE(ka) 5,3E+3. SE(kd) 5,3E-7
RU
70
60
50
40
30
20
10
0
-10
-200
0
200
400
600
800
1000
1200
1400
Time

Supplementary Figure 4. PNGase F treatment of purified 17T2 mAb. (A) Purified 17T2 mAb was incubated in the presence (+) or absence (–) of recombinant PNGase F and analyzed by SDS-PAGE. Red asterisks indicate the de-glycosylated product. **(B)** ELISA binding curves of serial dilutions of control treated 17T2 (red) and de-glycosylated 17T2 (blue) mAbs to recombinant SARS-CoV-2 RBD, coated at equimolar concentrations. Graph bars represent the average ± SD. **(C)** Neutralization curves of control treated 17T2 (red) and de-glycosylated 17T2 (blue) mAbs against ancestral SARS-CoV-2 WH1 variant. Values are mean +/- SD of duplicate samples. **(D)** The binding kinetics of de-glycosylated (left) and no de-glycosylated form of 17T2 mAb (right) to recombinant SARS-CoV-2 RBD were obtained using the BIAcore T100 system in single-cycle mode. mAbs were captured on the chip, and serial dilutions of RBD (WH1) were then injected over the chip surface. The K_D is labelled accordingly.

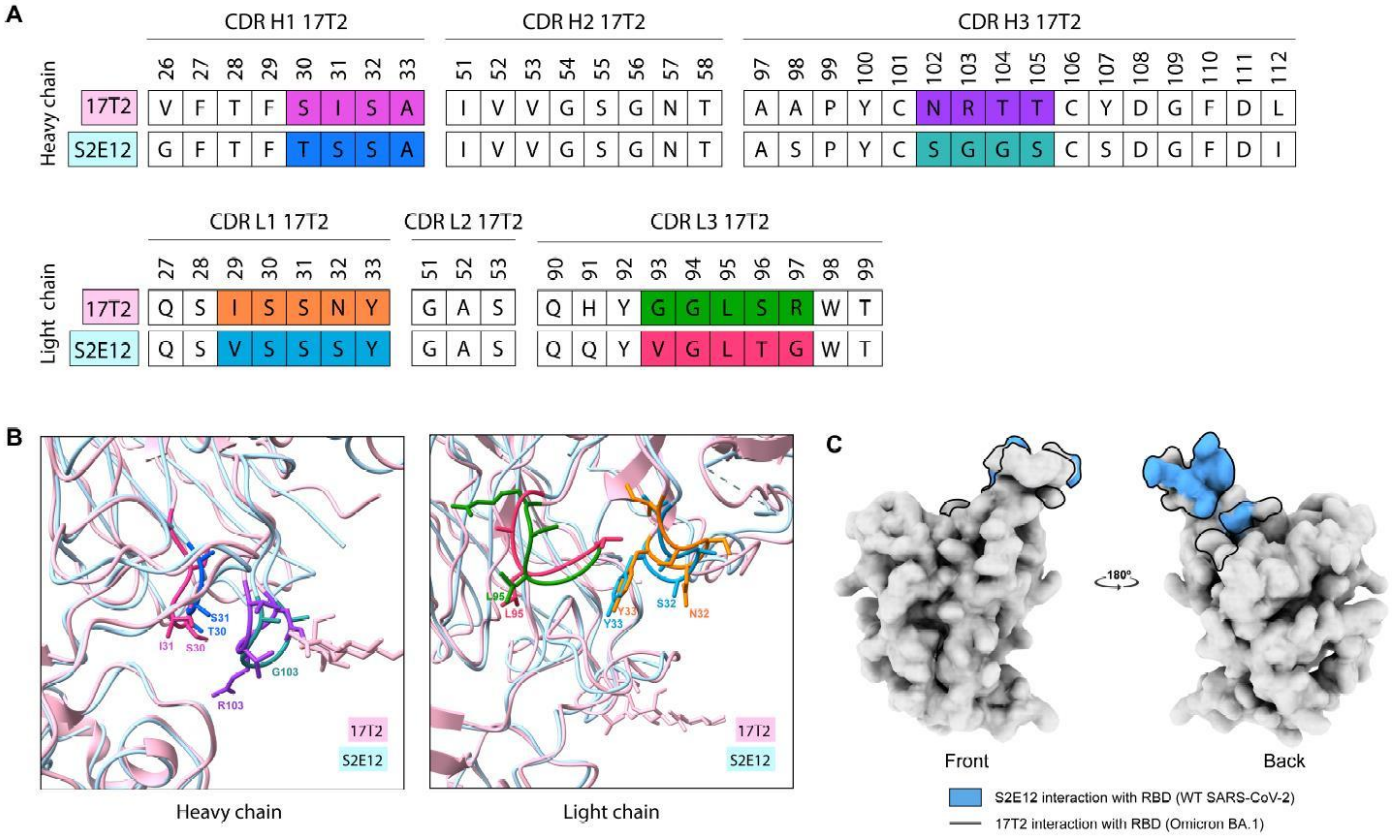
A
CDR H1 17T2
CDR H2 17T2
CDR H3 17T2
Heavy chain
26 27 28 29 30 31 32 33
51 52 53 54 55 56 57 58
97 98 99 100 101 102 103 104 105 106 107 108 109 110 111 112
17T2 V F T F S I S A I V V G S G N T A A P Y C N R T T C Y D G F D L
S2E12 G F T F T S S A I V V G S G N T A S P Y C S G G S C S D G F D I
CDR L1 17T2
CDR L2 17T2
CDR L3 17T2
Light chain
27 28 29 30 31 32 33
51 52 53
90 91 92 93 94 95 96 97 98 99
17T2 Q S I S S N Y G A S Q H Y G G L S R W T
S2E12 Q S V S S S Y G A S Q Q Y V G L T G W T
B
S31
T30
I31
S30
G103
R103
17T2
S2E12
Heavy chain
L95
L95
Y33
Y33
S32
N32
17T2
S2E12
Light chain
C
180°
Front
Back
S2E12 interaction with RBD (WT SARS-CoV-2)
17T2 interaction with RBD (Omicron BA.1)

Supplementary Figure 5. Comparative study of 17T2 Fab with similar antibody S2E12 Fab.

(A) Comparison of the sequences of the CDRs of both the heavy and light chains between the 17T2 and S2E12 antibodies, showing differences between residues with colors. **(B)** Alignment of the RBD-Fab structures of 17T2 and 2SE12 Fabs showing the side chains of the residues that are part of the regions with sequence differences (color codes as in **(A)**). **(C)** Different areas of interaction of 17T2 and S2E12 Fabs with the RBD of SARS-CoV-2 spike.

Supplementary Table 1. Phenotype and native isotype of the B cells originating the mAbs, and the antibody gene usage of the heavy and light chain variable regions.

Name	B cell of origin	
	B cell phenotype	Isotype
17T2	$CD19^{+}HLA\text{-}DR^{+}CD27^{+}IgA^{+}CD21^{+}IgM^{-}IgD^{-}lambda^{-}$	IgA
54T1	$CD19^{+}HLA\text{-}DR^{+}CD27^{+}IgA^{+}CD21^{+}IgM^{-}IgD^{-}lambda^{-}$	IgA
130T1	$CD19^{+}HLA\text{-}DR^{+}CD27^{+}IgA^{-}CD21^{+}IgM^{-}IgD^{-}lambda^{-}$	IgG
119T2	$CD19^{+}HLA\text{-}DR^{+}CD27^{+}IgA^{-}CD21^{+}IgM^{-}IgD^{-}lambda^{+}$	IgG
131T2	$CD19^{+}HLA\text{-}DR^{+}CD27^{+}IgA^{-}CD21^{+}IgM^{-}IgD^{-}lambda^{-}$	IgG

Name	IgHeavy			
	V call	D call	J call	% V identity
17T2	IGHV1-58*01	IGHD2-2*01,IGHD2-2*02,IGHD2-2*03	IGHJ3*01,IGHJ3*02	94,5
54T1	IGHV3-53*04	IGHD5-12*01	IGHJ6*02	96,6
130T1	IGHV1-46*01	IGHD5-18*01,IGHD5-5*01	IGHJ4*01,IGHJ4*02	96,6
119T2	IGHV3-9*01	IGHD2-15*01,IGHD2-21*01,IGHD2-21*02	IGHJ3*02	98
131T2	IGHV3-30*18,IGHV	IGHD5-18*01,IGHD5-5*01	IGHJ4*02	97,3

Name	IgLight			
	Chain	V call	J call	% V identity
17T2	Kappa	IGKV3-20*01	IGKJ1*01	96,5
54T1	Kappa	IGKV1-9*01	IGKJ1*01	98,6
130T1	Kappa	IGKV1-17*01	IGKJ1*01	98,6
119T2	Lambda	IGLV2-14*03	IGLJ3*02	98,3
131T2	Kappa	IGKV3-15*01	IGKJ4*01	97,6

Supplementary Table 2. Kinetic rate constants and affinities determined for the 17T2 mAb against SARS-CoV-2 RBD variants.

17T2			
SARS-CoV-2 RBD variants	**ka (1/Ms)**	**kd (1/s)[a]**	**K_D (nM)[b]**
WH1	2,62E+06	1,21E-4	0,0462
Alpha	9,61E+05	<1.0E-05	<0.1
Beta	2,30E+06	<1.0E-05	<0.1
Delta	3,32E+06	<1.0E-05	<0.1
Omicron BA.1	1,08E+07	<1.0E-05	<0.1
Omicron BA.2	5,90E+07	<1.0E-05	<0.1

a. For most of the Biacore experiments, no decay in the binding signal was observed during the time allowed for dissociation. According to the ‘‘5% rule’’, the k_d can be resolved only if 5% or more of the bound material dissociates. Therefore, the upper limit on the K_d (in 1/s) is given by $K_d < \ln(0.95)/td$, where td is the amount of time (in seconds) allowed for dissociation.

b. K_D based on the kd limit determined by the ‘‘5% rule.’’

Supplementary Table 3. Pseudovirus spike mutations relative to ancestral WH1.

Name	Mutations
D614G	D614G
Alpha	H69-70del, Y144del, N501Y, A570D, P681H, T716I, S982A and D1118H
Beta	L18F, D80S, D215G, L242-244del, R246I, K417N, E484K, N501Y, D614G, A701V
Gamma	L18F, T20N, P26S, D138Y, R190S, K417T, E484K, N501Y, D614G, H655Y, T1027I, V1176F
Delta	T19R, 157-158 del, L452R, T478K, D614G, P681R, D950N
Mu	T95I, Y144S, Y145N, R346K, E484K, N501Y, D614G, P681H, D950N
BA.1	A67V, H69-70del, T95I, G142D, V143-145del, N211del, L212I, ins214EPE, G339D, S371L, S373P, S375F, K417N, N440K, G446S, S477N, T478K, E484A, Q493R, G496S, Q498R, N501Y, Y505H, T547K, D614G, H655Y, N679K, P681H, N764K, D796Y, N856K, Q954H, N969K, L981F
BA.2	T19I, L24S, P25-27del, G142D, V213G, G339D, S371F, S373P, S375F, T376A, D405N, R408S, K417N, N440K, S477N, T478K, E484A, Q493R, Q498R, N501Y, Y505H, D614G, H655Y, N679K, P681H, N764K, D796Y, Q954H, N969K
BA.4/5	T19I, L24S, P25-27del, H69-70del, G142D, V213G, G339D, S371F, S373P, S375F, T376A, D405N, R408S, K417N, N440K, L452R, S477N, T478K, E484A, F486V, Q498R, N501Y, Y505H, D614G, H655Y, N679K, P681H, N764K, D796Y, Q954H, N969K
BQ.1.1	T19I, L24S, P25-27del, H69-70del, G142D, V213G, G339D, R346T, S371F, S373P, S375F, T376A, D405N, R408S, K417N, N440K, K444T, L452R, N460K, S477N, T478K, E484A, F486V, Q498R, N501Y, Y505H, D614G, H655Y, N679K, P681H, N764K, D796Y, Q954H, N969K

Supplementary Table 4. Representation of reported SARS-CoV-2 RBD mutations in key variants. Color highlighted boxes show the presence of RBD mutations in each SARS-CoV-2 variant (same color codes as in **Figure 3F**).

		Receptor-binding-domain mutations																						
		339	346	371	373	375	376	405	408	417	440	444	446	452	460	477	478	484	486	490	493	496	498	501	505
WT Sars-Cov-2		G	R	S	S	S	T	D	R	K	N	K	G	L	N	S	T	E	F	F	Q	G	Q	N	Y
Alpha	B.1.1.7																							Y	
Beta	B.1.351									N								K						Y	
Gamma	P.1									T								K						Y	
Delta	B.1.617.2													R			K								
Epsilon	B.1.427/9													R											
Zeta	P.2																	K							
Eta	B.1.525																	K							
Theta	P.3																	K						Y	
Iota	B.1.526																	K							
Kappa	B.1.617.1													R			K	Q							
Lambda	C.37													Q						S					
Mu	B.1.621		K															K						Y	
Omicron	BA.1	D		L	P	F				N	K		S			N	K	A			R	S	R	Y	H
	BA.2	D		F	P	F	A	N	S	N	K					N	K	A			R		R	Y	H
	BA.4/BA.5	D		F	P	F	A	N	S	N	K			R		N	K	A	V				R	Y	H
	BQ.1.1	D		F	P	F	A	N	S	N	K	T		R	K	N	K	A	V				R	Y	H

Supplementary Table 5. RBD/17T2 Fab model refinement and statistic.

Model	RBD-Fab	
Composition (#)		
Chains	3	
Atoms	5106 (Hydrogens: 0)	
Residues	Protein: 652 Nucleotide: 0	
Water	0	
Ligands	NAG: 4	
Bonds (RMSD)		
Length (Å) (# > 4σ)	0.006 (0)	
Angles (°) (# > 4σ)	1.208 (10)	
MolProbity score	2.47	
Clash score	25.75	
Ramachandran plot (%)		
Outliers	0.31	
Allowed	10.37	
Favored	89.32	
Rotamer outliers (%)	0.71	
Cβ outliers (%)	0.00	
Peptide plane (%)		
Cis proline/general	5.4/0.2	
Twisted proline/general	0.0/0.0	
CaBLAM outliers (%)	5.00	
ADP (B-factors)		
Iso/Aniso (#)	5106/0	
min/max/mean		
Protein	23.54/440.00/243.00	
Nucleotide	---	
Ligand	106.97/440.00/301.85	
Water	---	
Occupancy		
Mean	1.00	
occ = 1 (%)	100.00	
0 < occ < 1 (%)	0.00	
occ > 1 (%)	0.00	
Data		
Box		
Lengths (Å)	60.40, 66.15, 119.70	
Angles (°)	90.00, 90.00, 90.00	
Supplied Resolution (Å)	3.5	
Resolution Estimates (Å)	Masked	Unmasked
d FSC (half maps; 0.143)	3.6	3.8
d 99 (full/half1/half2)	2.4/5.5/5.5	2.4/5.1/5.1
d model	2.0	2.0
d FSC model (0/0.143/0.5)	1.9/2.6/3.5	1.9/2.6/3.5
Map min/max/mean	-1.27/1.54/0.01	
Model vs. Data		
CC (mask)	0.78	
CC (box)	0.79	
CC (peaks)	0.79	
CC (volume)	0.78	
Mean CC for ligands	0.84	